Instability of the high-pressure CsCl structure in most III-V semiconductors

Kwiseon Kim, V. Ozoliņš,* and Alex Zunger
National Renewable Energy Laboratory, Golden, Colorado 80401
(Received 24 May 1999)

Using the density-functional linear response method, we study dynamical instabilities of the high-pressure CsCl phase in III-V semiconductors. For InSb, we find no phonon instability that could prevent the CsCl phase from forming, consistent with the experimental observation. In contrast, for the more ionic GaP, GaAs, InP, and InAs, we find that, while statically stable, the CsCl phase is dynamically unstable at high pressures with respect to transverse-acoustic $[\xi\xi 0]$ phonons. Analysis of the soft normal modes via ''isotropy subgroup'' suggests two candidate structures that will replace CsCl structure at high pressure: the tP4 (B10) InBi type and the oP4 (B19) AuCd type. Experimental examination of these predictions is called for.
[S0163-1829(99)50836-9]

The classic thinking on the phase stability of covalent zinc-blende semiconductors suggests[1–3] that as pressure is applied these phases transform into crystal structures that exist at zero pressure in more ionic $A^{(n)}B^{(8-n)}$ octet compounds. Thus, as pressure is increased, zinc-blende III-V semiconductors are expected to transform into the NaCl structure or the CsCl structure. This expectation has guided many theoretical calculations[4,5] that have searched and found the zinc-blende $\rightarrow$NaCl $\rightarrow\beta$-Sn$\rightarrow$CsCl transition sequence. These calculations have used the ''standard methodology,'' of first guessing a few candidate high-pressure phases, then computing their total energies vs volume, from which the enthalpies $H=E-PV$ and the transition pressures P_c between phases α and β are obtained via $H_\alpha=H_\beta$. Figure 1 illustrates the results of such static total-energy calculations performed within the pseudopotential framework[6–8] for InP and InSb, showing the predicted sequence of phases. While it was first believed, to the best of our knowledge, that such calculations[4,5] agreed with experiments, recent advent of high-pressure angle-dispersive x-ray diffraction techniques[9] has revealed that the previous assignments of the NaCl structure to III-V compounds other than InP, InAs, and nitrides were incorrect.[10] Instead, the observed high-pressure phases exhibit fundamentally new structures, with larger unit cells and lower symmetries than simple text-book structures such as NaCl or β-Sn. While these new structures were later confirmed via total-energy calculations[5] (that used the observed structures as input), these experimental discoveries[10] exposed a weakness in our current theoretical approach for predicting high-pressure phases by guessing the candidate structures at the outset. Indeed, this method of ''rounding up the usual suspects'' has serious shortcomings: (i) it may miss unsuspected, yet more stable structures, and/or (ii) result in theoretically predicted transitions that are unphysical because the predicted phases could be dynamically unstable. Recent *dynamic* phonon calculations explained[11] the *systematic absence* of the high-pressure NaCl phase of covalent semiconductors in terms of a generic TA(X) phonon instability overlooked by static calculations.

Here we investigate the stability of the high-pressure CsCl phase of octet III-V semiconductors. This structure has been proposed theoretically[4,5] for GaP, GaAs, InP, InAs, and InSb and experimentally[12–14] for GaSb, InSb, and HgTe. We demonstrate here that (i) while standard static calculations (e.g., Fig. 1) show that this phase is universally stable at high pressures for many III-V compounds, (ii) dynamic phonon calculations for the CsCl structure show that this phase has phonon instabilities that prevent its formation for GaP, GaAs, InP, and InAs. (iii) From symmetry analysis of the soft phonon modes we propose two high-pressure structures that replace the CsCl phase in the high-pressure phase diagrams of III-V semiconductors: (i) the oP4 (AuCd structure-type) with space group $Pmma$, and (ii) the tP4 (InBi structure type) with space group $P4/nmm$.

Initial inquiries into potential instabilities of a presumed phase (e.g., CsCl) can be conducted via static total-energy calculations examining the response to unit-cell and frozen-in phonon distortions that have been found to be unstable in similar systems (e.g., bcc metals). For instance, Fig. 2(a) shows the total energy of InP for deformations carrying the bcc-based B2 (CsCl) structure into the hcp-based B19 (AuCd) structure via a tetragonal elastic shear in the [001] direction, followed by a shuffle of CsCl (110) planes along

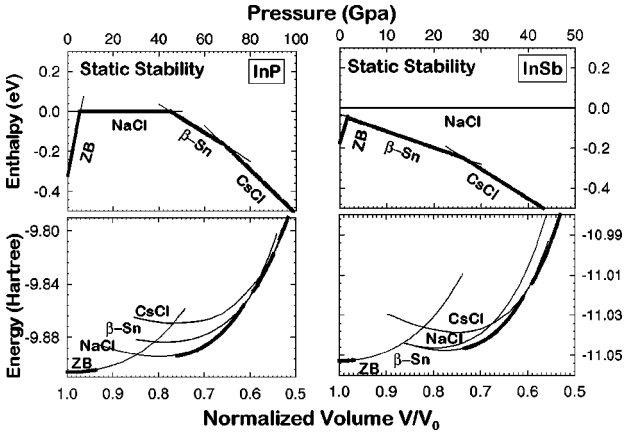

FIG. 1. Static stability curves for InP and InSb in the assumed zinc-blende (ZB), NaCl, β-Sn, and CsCl structures. Top curves: the enthalpies $E-PV$, showing the transition pressures as a crossing between two enthalpy lines. Bottom curves: total energies vs volume. V_0 is the calculated equilibrium volume for the zinc-blende structure. The bold lines in the E vs V curves denote volume ranges where static stability is predicted.

 ©1999 The American Physical Society

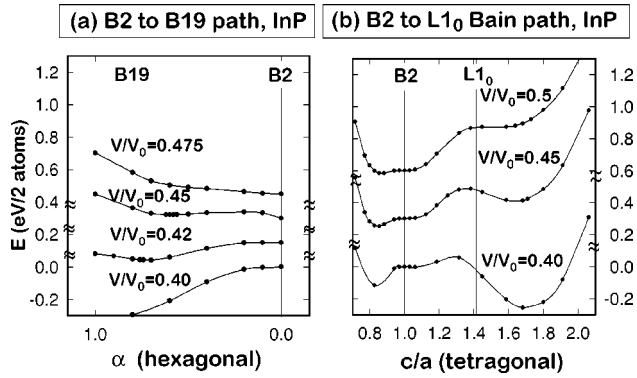

FIG. 2. Total-energy change due to distortions of the B2 (CsCl) structure of InP. (a) The B2→B19 path. $\alpha=0$ for the undistorted B2 structure and $\alpha=1$ when $c/a=\sqrt{2/3}$ and the shift of planes $\delta=\sqrt{3}/6a_{\rm bcc}$. (See text.) (b) The B2 →L1$_0$ path.

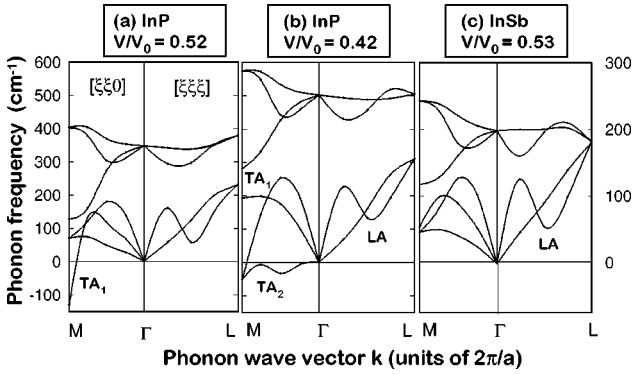

FIG. 3. Phonon-dispersion curves in the B2 structure of (a) InP and (b) InSb at a few normalized volumes V/V_0. Imaginary phonon frequencies are shown as negative.

$[1\bar{1}0]$. We see that such distortions result in a lower energy phase when the volume V/V_0 (where V_0 is the theoretical equilibrium volume in zinc-blende phase,) is smaller than about 0.42. This is still in the volume regime where static calculations of the type shown in Fig. 1 predict a stable CsCl phase. Figure 2(b) shows the total-energy changes due to tetragonal c/a distortions, carrying the B2 (CsCl) structure (cubic symmetry) to the L1$_0$ (CuAu) structure (tetragonal symmetry). We see that here too the B2 structure is unstable in the volume range $V/V_0=0.40-0.55$. As the volume is decreased below $V/V_0=0.45$, a second minimum around $c/a=1.7$ appears. The shear modulus $C_s=(C_{11}-C_{12})/2$ of the CsCl structure, given by the curvature of the total energy around $c/a=1$ in Fig.2(b), becomes soft when V/V_0 is below 0.45. The velocity of a $[1\bar{1}0]$-polarized shear wave propagating along the [110] direction is given[15] by $V_{s[1\bar{1}0]}=[(C_{11}-C_{12})/2\rho]^{1/2}$, where ρ is the mass density. Thus, the softening of the shear modulus indicates a corresponding softening of acoustic phonon mode along the [110] direction with atomic displacements polarized in the $[1\bar{1}0]$ direction. Results similar to those shown in Fig. 2 for InP were obtained for InAs showing its instability in the B2 structure. However, for InSb, the B2 structure was stable with respect to both distortions.

We thus see that even though static total-energy calculations of hydrostatic compression suggest the stability of the assumed B2 structure of InP and InAs in some volume range, nonhydrostatic strain (Fig. 2) clearly demonstrates that this phase is unstable in these volume ranges. While calculations such as those illustrated in Fig. 2 can demonstrate that a *postulated phase* (here, B2) is not a viable candidate for equilibrium, such methods do not show a systematic way of finding potential instabilities and do not point to the phase that replaces the unstable one. To address these two issues we take the following course: (a) calculate the phonon spectrum of the *postulated phase*, searching for specific unstable vibrational modes, (b) use group theoretical analysis (''isotropy subgroups,'' see below) to identify the possible lower symmetry phases, and then (c) perform static total-energy calculations to optimize the structure predicted from the soft modes.

The phonon dispersion is calculated[16] using the density-functional linear response method.[17] Figure 3 shows the phonon dispersion curves for InP and InSb in the B2 structure at volumes where, according to the static total-energy calculation shown in Fig. 1, this structure is stable. We find that in InP two transverse-acoustic (TA) modes along the $k=[\xi\xi0]$ direction are unstable ($\nu^2<0$). The degree of instability [as measured by the magnitude of $-\nu^2(k)$] is most severe at the zone boundary M point corresponding to $k=(1/2,1/2,0)$. The symmetry group of this wave vector is $4/mmm$, and the allowed irreducible representations are M_2^-, M_3^-, and $2M_5^-$. These include two degenerate acoustic modes (M_5^-) and two degenerate optic modes (M_5^-), in addition to a nondegenerate acoustic mode (M_2^-) and an optic mode[18] (M_3^-). From an inspection of the eigenvectors of the unstable mode, we find that they belong to the TA$_1$(M_2^-) and TA$_2$(M_5^-) representations. Repeating the phonon dispersion calculations over a range of unit-cell volumes where the B2 phase is statically stable (Fig. 1), shows that for InP, the TA$_1$(M_2^-) mode is unstable below a pressure of 100 GPa ($V/V_0=0.50$), while the TA$_2$(M_5^-) mode becomes unstable above a pressure of 160 GPa ($V/V_0=0.44$). For InAs, the two pressures are 57 GPa ($V/V_0=0.55$) and 135 GPa ($V/V_0=0.45$), while InSb shows none of these anomalies in the pressure range where the B2 phase is statically stable. Thus, our phonon calculation predicts that the B2 phase will not occur in InP, GaP, GaAs, and InAs, but it could occur in InSb.

We next describe how the ''isotropy subgroup'' analysis can be used to narrow down the range of structures that will replace the phonon-unstable B2 structure. The eigenfuctions for the soft modes TA$_1$(M_2^-) and TA$_2$(M_5^-) are depicted in Fig. 4(a) and Fig. 5(a), respectively. We see that the TA$_1$(M_2^-) mode is polarized along the [001] direction, while the TA$_2$(M_5^-) mode displacements are in the $[1\bar{1}0]$ direction. Having identified the symmetries TA$_1$(M_2^-) and TA$_2$(M_5^-) of soft modes, we consider the corresponding modes as order parameters in a pressure-induced phase transition that can be described by the Landau expansion of the enthalpy function. During a second-order phase transition where the original symmetry is lowered by a continuous structural distortion, the new symmetry must leave the distortion invariant. Thus, there is a group/subgroup relation between the undeformed/deformed phases. Such a subgroup is called an ''isotropy subgroup.''[19] The allowed isotropy subgroups for each space group and for given order param-

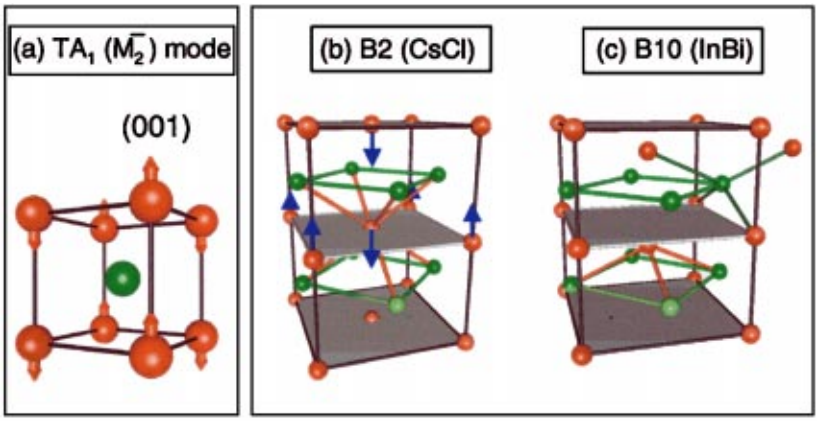

FIG. 4. (Color) TA$_1$(M_2^-) derived structure from the B2 (CsCl) starting point: (a) The phonon eigenmode. (b) The undistorted B2 structure. Arrows denote displacements of anions (red) leading to (c) the B10 structure.

eter irreducible representations are compiled by Stokes and Hatch.[19] There are 6 isotropy subgroups for M_2^- and 26 subgroups for M_5^-. Using the isotropy subgroup table,[19] it is easy to identify the structure type for each case (Table I). For the sake of simplicity, we now confine ourselves to those subgroups called ''maximal isotropy subgroups.''[18] For M_2^-, there are three [first three rows (1-3) in Table I], while for M_5^-, there are seven such sets [the seventh to thirteenth rows (1-7) in Table I].

(i) M_2^- mode and the B10 crystal structure. Figure 4(c) gives the crystal structure that will result from one of the highest symmetry members of the unstable M_2^- mode. The new structure has $P4/nmm$ symmetry. This is the tP4, InBi-type[21] structure (B10) derived by a soft M_2^- mode. In this structure two In atoms are in one (100) plane, and two P atoms are at two different (100) planes, separated by $(1-2z)c/a$, where z is a dimensionless cell-internal parameter. In the undistorted B2 structure [Fig. 4(b)] each anion (shown in red) has four nearest-neighbor cations (shown in green) on each side of the shaded (001) plane. In the distorted tP4 structure [Fig. 4(c)], the anions are displaced in the [001] direction (see blue arrows) so that now each anion has four nearest-neighbor cations at a distance $R_{\mathrm{In}-X}^{(1)}=a\{[(c/a)z]^2+1/4\}^{1/2}$ forming a square to one side of the (001) plane, and four additional next nearest neighbors at a distance $R_{\mathrm{In}-X}^{(2)}=a\{[(c/a)(1-z)]^2+1/4\}^{1/2}$. When $z\rightarrow 1/2$ and $c/a\rightarrow 1/\sqrt{2}$ then $R_{\mathrm{In}-X}^{(1)}=R_{\mathrm{In}-X}^{(2)}$, thus restoring the eightfold coordinated B2 structure.

(ii) M_5^- mode and the B19 crystal structure: Figure 5(c) gives the B19 crystal structure derived from the M_5^- mode. This orthorhombic structure has $Pmma$ symmetry and can be considered as a distorted diatomic hcp structure. The B2 structure transforms into this structure when (a) the hexagonal B2 faces [the (110) plane shown as top view at the bottom of Fig. 5] become regular hexagons and (b) the second (110) layer of atoms are placed at the center of the triangles. That is, the b/a ratio becomes $1/\sqrt{3}$ rather than $1/\sqrt{2}$ in the B2 structure and the atoms in alternate (110) planes shifts $\sqrt{3}/6a_{\mathrm{bcc}}$ in the $[1\bar{1}0]$ direction as shown with arrows, making it an ideal hcp stacking as shown in Fig. 5(c). In practice, due to orthorhombic symmetry, in general, $b/a\neq 1/\sqrt{3}$ and the shift $\delta\neq\sqrt{3}/6a_{\mathrm{bcc}}$.

Having identified, via a symmetry analysis of the B2 soft modes, B10 and B19 as candidate structures that can replace the B2 stucture [Figs. 4(c) and 5(c)], we now compute the static total energies of InP in these structures, relaxing the cell-internal and cell-external structural parameters allowed by symmetry. We find that both the B10 and the B19 phases are lower in energy than the B2 phase at the volumes where the B2 is expected to be stable according to hydrostatic calculations alone (Fig. 1). Near the transition pressure into the B2 phase, B10 is the lowest energy phase. At $V/V_0=0.50$, the total energy of the B10 phase is lower than that of the B2 phase by 29 meV and B19 is lower by 1 meV. As the pressure is raised further, B19 becomes the lowest energy structure. At $V/V_0=0.42$, the total-energy differences are -73

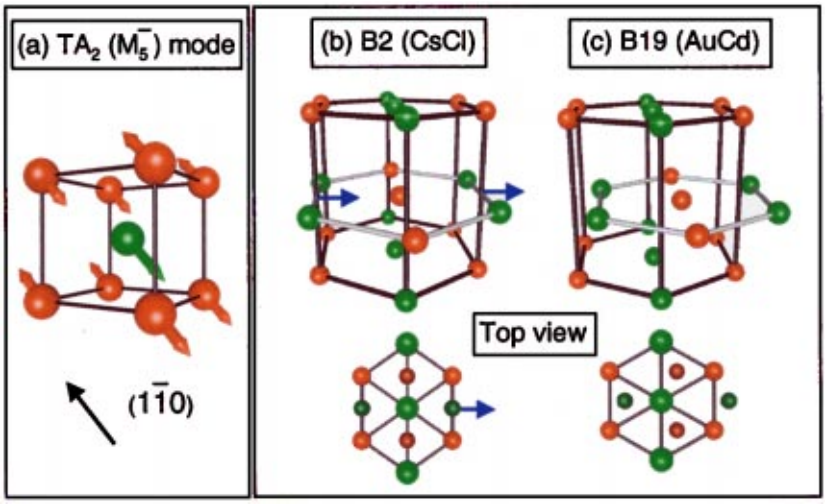

FIG. 5. (Color) TA$_1$(M_5^-) derived structure from the B2 (CsCl) starting point: (a) The phonon eigenmode. (b) The undistorted B2 structure. Arrows denote the displacement of atoms on alternating (110) planes leading to (c) the B19 structure.

TABLE I. Isotropy subgroups of the parent CsCl structure ($Pm\bar{3}m;O_h^1$) that corresponds to the M_2^- and M_5^- order parameters. Atomic positions are given in terms of Wyckoff notation. In parentheses we give the pages in Ref. 20 where the positions are given. The maximal symmetry isotropy subgroups are the first three rows (1-3) for M_2^-, and the first seven rows (1-7) for M_5^-.

	Subgroup	Basis vectors	Atomic positions (page no.)	Structure type	Example
			Irrep = $TA_1(M_2^-)$		
(1)	$P4/nmm(D_{4h}^7)$	$(1,1,0),(\bar{1},1,0),(0,0,1)$	$2a;2c$ (439)	tP4 (B10)	InBi, BaO, PbO, FeS
(2)	$I4/mcm(D_{4h}^{18})$	$(0,0,2),(2,0,0),(0,2,0)$	$8g;8h$ (471)	tI16	
(3)	$I\bar{4}3m(T_d^3)$	$(2,0,0),(0,2,0),(0,0,2)$	$2a;6b;8c$ (653)	cI16	S_4Tl_3V
(4)	$Ibam(D_{2h}^{26})$	$(0,0,2),(2,0,0),(0,2,0)$	$4a;4b;8j$ (317)	oI16	
(5)	$I\bar{4}2m(D_{2d}^{11})$	$(0,0,2),(2,0,0),(0,2,0)$	$2a;2b;4c;8i$ (417)	tI16	
(6)	$I222(D_2^8)$	$(2,0,0),(0,2,0),(0,0,2)$	$2a;2b;2c;2d;8k$ (205)	oI16	
			Irrep = $TA_2(M_5^-)$		
(1)	$Pmma(D_{2h}^5)$	$(1,0,\bar{1}),(0,1,0),(1,0,1)$	$2e;2f$ (265)	oP4 (B19)	AuCd, CdMg, IrW, NbPt
(2)	$Cmmm(D_{2h}^{19})$	$(0,0,2),(2,0,0),(0,1,0)$	$4h;4i$ (295)	oC8	
(3)	$R3m(C_{3v}^5)$	$(\bar{2},2,0),(0,\bar{2},2),(1,1,1)$	$3a;9b;3a;9b$ (519)	hR8	
(4)	$R32(D_3^7)$	$(\bar{2},2,0),(0,\bar{2},2),(1,1,1)$	$3a;9d;3b;9e$ (507)	hR8	
(5)	$I4/mmm(D_{4h}^{17})$	$(0,2,0),(0,0,2),(2,0,0)$	$4d;4e;8h$ (469)	tI16	Ag_3InLa_4
(6)	$I4/mmm(D_{4h}^{17})$	$(2,0,0),(0,2,0),(0,0,2)$	$4d;4e;8h$ (469)	tI16	Ag_3InLa_4
(7)	$I2_13(T^5)$	$(2,0,0),(0,2,0),(0,0,2)$	$8a;8a$ (603)	cI16	CoU
(8-26)	$P2/m(C_{2h}^1)$, $Imma(D_{2h}^{28})$, $Immm(D_{2h}^{25})$, $Immm(D_{2h}^{25})$, $C2/m(C_{2h}^3)$, $Fmm2(C_{2v}^{18})$, $Fmm2(C_{2v}^{18})$, $R3(C_3^4)$, $C2/m(C_{2h}^3)$ $C2/m(C_{2h}^3)$, $Cm(C_s^3)$, $C2(C_2^3)$, $I2_12_12_1(D_2^9)$, $Imm2(C_{2v}^{20})$, $P\bar{1}(C_i^1)$, $C2(C_2^3)$, $Cm(C_s^3)$, $Cm(C_s^3)$, $P1(C_1^1)$				

meV between B10 and B2 and -92 meV between B19 and B2.

In conclusion, we found that the CsCl structure is dynamically unstable for InP as well as for GaP, GaAs, and InAs. For InP, it could be replaced by the B10 and the B19 structures while other structural modifications are possible[18] (Table I), the general method we have outlined is capable of finding the stablest. For InSb, our calculations show no instability, which is consistent with experimental observation of the B2 (or disordered bcc) phase.[13] Experimental searches for the proposed B10 and B19 crystal structures are called for.

This work was supported by Basic Energy Sciences, Division of Materials Science, under Contract No. DE-AC36-98-GO10337.

*Present address: Sandia National Laboratories, Livermore, CA 94551-0969.

[1] J. C. Phillips, *Bonds and Bands in Semiconductors* (Academic Press, New York, 1973), p. 200.

[2] E. Mooser and W. B. Pearson, Acta Crystallogr. **A12**, 1015 (1959).

[3] E. Parthé, *Crystal Chemistry of Tetrahedral Structures* (Gordon and Breach, New York, 1964).

[4] S. Froyen and M. L. Cohen, Phys. Rev. B **28**, 3258 (1983); S. B. Zhang and M. L. Cohen, *ibid.* **35**, 7604 (1987); A. Garcia and M. L. Cohen, *ibid.* **47**, 6751 (1993).

[5] A. Mujica and R. J. Needs, Phys. Rev. B **55**, 9659 (1997); P. Rodríguez-Hernández *et al.*, Phys. Status Solidi B **198**, 455 (1996); A. Mujica *et al.*, Phys. Rev. B **52**, 8881 (1995).

[6] J. Ihm, A. Zunger, and M. L. Cohen, J. Phys. C **12**, 4409 (1979).

[7] We used optimized pseudopotentials generated according to the method of A. M. Rappe, K. M. Rabe, E. Kaxiras, and J. D. Joannopoulos, Phys. Rev. B **41**, 1227 (1990).

[8] We used the exchange-correlation fuctional of J. P. Perdew and A. Zunger, Phys. Rev. B **23**, 5048 (1981).

[9] R. J. Nelmes and M. I. McMahon, J. Synchrotron Radiat. **1**, 69 (1994).

[10] M. I. McMahon and R. J. Nelmes, J. Phys. Chem. Solids **56**, 485 (1995); **56**, 539 (1995); **56**, 545 (1995); Phys. Status Solidi B **198**, 389 (1996).

[11] V. Ozoliņš and A. Zunger, Phys. Rev. Lett. **82**, 767 (1999).

[12] R. J. Nelmes and M. I. McMahon, in *High Pressure in Semiconductor Physics I*, edited by T. Suski and W. Paul, Semiconductors and Semimetals Vol. 54, edited by R. K. Willardson and E. R. Weber (Academic Press, New York, 1998).

[13] C. A. Vanderborgh *et al.*, Phys. Rev. B **40**, 12 450 (1989); R. J. Nelmes and M. I. McMahon, Phys. Rev. Lett. **77**, 663 (1996).

[14] T. Huang and A. L. Ruoff, Phys. Rev. B **31**, 5976 (1985); R. J. Nelmes *et al.*, J. Phys. Chem. Solids **56**, 545 (1995).

[15] A. Auld, *Acoustic Fields and Waves in Solids* (Wiley, New York, 1973), Vol. 1.

[16] The first local-density approximation phonon calculations using the frozen-phonon method was done by J. Ihm *et al.*, Solid State Commun. **37**, 491 (1981). More recently linear response method (Ref. 17) has been developed.

[17] S. Baroni *et al.*, Phys. Rev. Lett. **58**, 1861 (1987).

[18] A. Saxena *et al.*, Phase Transit. **46**, 89 (1994). Studying the ''maximal isotropy'' subgroups alone is an approximation. In principle, all 26 subgroups should be examined.

[19] H. T. Stokes and D. M. Hatch, *Isotropy Subgroups of the 230 Crystallographic Space Groups* (World Scientific, Singapore, 1988), pp. I-347.

[20] *International Tables for Crystallography*, edited by T. Hahn (D. Reidel Publishing Co., Dordrecht, 1983), Vol. A.

[21] W. P. Binnie, Acta Crystallogr. **9**, 686 (1956); T. J. White *et al.*, J. Appl. Phys. **46**, 11 (1975).